AIAA JOURNAL
Vol. 36, No. 11, November 1998

Control of Flow-Induced Noise Behind a Circular Cylinder Using Splitter Plates

Donghyun You,* Haecheon Choi,† Myung-Ryul Choi,* and Shin-Hyoung Kang‡
Seoul National University, Seoul 151-742, Republic of Korea

Laminar vortex sheddings behind a circular cylinder with and without splitter plates attached to the cylinder base at the Reynolds numbers of 100 and 160 are simulated by solving the unsteady two-dimensional incompressible Navier–Stokes equations. The Strouhal number, lift, and drag rapidly change with the length of the splitter plate. Acoustic source functions are obtained from the computed near-field velocity and pressure using the Curle's solution of the Lighthill acoustic analogy. In the case of no splitter plate, the volume quadrupole noise is small at a low Mach number, compared with the surface dipole noise from the cylinder. When a splitter plate is attached to the cylinder, there are significant modifications of the dipole and quadrupole sources. Changes in the noise sources at $Re = 100$ are very different from those at $Re = 160$, and their differences are closely related to the secondary vortex generated at the tip of the splitter plate. Scattering effects at the edge of the splitter plate are also considered.

Nomenclature

c = sound speed
$\dot{D}_i$ = dipole source function
d = cylinder diameter
f = vortex shedding frequency
G = Green's function of the scattering problem
$\hat{G}$ = Fourier-transformed Green's function of the scattering problem
k = wave number, ω/c_∞
l = length of the splitter plate
M = freestream Mach number, u_∞/c_∞
n_j = directional cosine of the outward normal to a solid surface
P_{ij} = $p\delta_{ij} - \tau_{ij}$
p = pressure
$\ddot{Q}_{ij}$ = quadrupole source function
Q_s = scattering source function generated by the distribution of Lighthill stresses near the plate edge
R = distance between an observation point and the plate edge
Re = freestream Reynolds number, $u_\infty d/\nu$
r = distance between observation and source points, $|\boldsymbol{r}| = |\boldsymbol{x} - \boldsymbol{y}|$
r_s = integration radius from the edge of the splitter plate [Eq. (14)]
r_0 = distance between a source point and the plate edge
Sr = Strouhal number, fd/u_∞
T_{ij} = Lighthill stress tensor
t = time
t^* = retarded time, $t - Mx\cosh\xi$; Eq. (8)
u_i = velocity in x_i
x = $|\boldsymbol{x}|$
$\boldsymbol{x}$ = observation point position vector
x_i = Cartesian coordinates
$\boldsymbol{y}$ = source point position vector
δ = Dirac's delta function
δ_{ij} = Kronecker delta
$\partial\Omega$ = cylinder surface
θ = angle of an observation point from x_1 axis
θ_0 = angle of a source point from x_1 axis
ν = kinematic viscosity
ξ = integration variable of the Hankel function
ρ = fluid density
$\rho_c - 1$ = acoustic density fluctuations in the far field due to dipole and quadrupole radiation
$\rho_s - 1$ = acoustic density fluctuations in the far field due to scattering radiation
τ_{ij} = viscous stress tensor
Ω = computational domain
ω = vorticity; frequency
$[\,]$ = function evaluated at the retarded time; $[f]$ is equal to $f(t - MR)$

Subscript

∞ = freestream quantity

I. Introduction

VORTEX shedding observed in the wake behind a circular cylinder increases drag on the cylinder, and the body suffers from the periodic force in the direction normal to the mainstream. Also, the main sources of the flow-induced noise behind a bluff body are the drag and lift fluctuations and the disturbed unsteady velocity fluctuations in the wake region. The drag and lift fluctuations on the body generate a dipole characteristic noise, and unsteady wake generates a quadrupole characteristic noise. Therefore, control methods reducing the mean drag on the body may also reduce the drag and lift fluctuations and, thus, reduce the flow-induced noise.

Much research has been focused on control of vortex shedding with active and/or passive means from the viewpoint of flow modification. Among them, the splitter plate attached to the cylinder base has been one of the most successful devices that control vortex shedding behind a cylinder. An interesting observation from the control of vortex shedding using the splitter plate at high Reynolds numbers [$\sim\mathcal{O}(10^4)$] is that the vortex shedding frequency does not decrease monotonically as the length of the splitter plate increases; the shedding frequency decreases for $l < d$ and increases for $d < l < 2d$, and then it decreases as the length of the plate further increases.[1–4] Therefore, the noise generated from the drag and lift fluctuations on the cylinder and the velocity fluctuations in the wake may also show a nonmonotonic behavior as the length of the plate increases.

Recently, Kwon and Choi[5] investigated the effect of the splitter plate on laminar vortex shedding behind a circular cylinder at Reynolds numbers of 80–160. They showed that for $Re \geq 120$ the shedding frequency changed similarly as just described, whereas for $Re \leq 100$ the shedding frequency monotonically decreased as the plate length increased. They attributed the increased shedding

Received June 25, 1997; revision received March 5, 1998; accepted for publication July 21, 1998.

*Graduate Student, Department of Mechanical Engineering.
†Assistant Professor, Department of Mechanical Engineering. E-mail: choi@socrates.snu.ac.kr. Member AIAA.
‡Professor, Department of Mechanical Engineering.

frequency at $l > d$ in the case of $Re \geq 120$ to a generation of the secondary vortex at the tip of the splitter plate. This secondary vortex near the tip of the splitter plate may also be a strong source of the flow-induced noise.

Lighthill[6] formulated a linear, inhomogeneous wave equation from the exact equations of fluid motion and showed that an unsteady flow region in an unbounded domain is acoustically equivalent to a distribution of quadrupole sources. When a solid body is present in the flow, Curle's integral solution[7] to the Lighthill equation provides a theoretical framework for predicting the noise of flow–body interaction. Using the acoustic analogy, at a low Mach number, the near-flowfield information is numerically obtained by solving the unsteady incompressible Navier–Stokes equations with the compressibility effect of $\mathcal{O}(M^2)$, and the information is used to compute the far-field acoustic density fluctuations. On the other hand, it is known that the scattering noise field is generated by acoustic interaction with the sharp edge. Crighton and Leppington[8,9] considered the scattering noise at a semi-infinite plane and solved this problem using the Wiener–Hopf technique. They reported that the dominant scattering effect occurs by the quadrupoles located very close to the edge.

The purpose of this study is to investigate the effect of the splitter plate on the flow-induced noise behind a circular cylinder using a numerical method. The Reynolds numbers used in this study are $Re = 100$ and 160; according to the results by Kwon and Choi,[5] variations of the vortex shedding frequency with respect to the splitter plate are very different at these two Reynolds numbers. We first simulate flow behind a circular cylinder without a splitter plate and compute the flow-induced noise sources using the acoustic analogies developed by Lighthill[6] and Curle.[7] Second, we conduct simulations at the same Reynolds numbers with splitter plates attached on the cylinder base. Modified noise sources will be investigated in detail with the observation of the flowfield changes. Also, the scattering effect generated by the secondary vortex at the tip of the splitter plate is considered. Computational details and the acoustic analogies are addressed in Secs. II and III, respectively. Results of the flowfield and noise source modifications are given in Sec. IV, followed by a summary in Sec. V.

II. Computational Details

The unsteady near flowfield and the radiated far sound field behind a circular cylinder in a two-dimensional uniform flow are considered. From the Lighthill acoustic analogy,[6] the acoustic source functions in the near field can be obtained by solving the incompressible Navier–Stokes equations. Thus, in the near field, the governing equations for an unsteady incompressible flow can be written in dimensionless form:

$$\frac{\partial u_i}{\partial t} + \frac{\partial}{\partial x_j} u_i u_j = -\frac{\partial p}{\partial x_i} + \frac{1}{Re} \frac{\partial}{\partial x_j} \frac{\partial u_i}{\partial x_j} \tag{1}$$

$$\frac{\partial u_i}{\partial x_i} = 0 \tag{2}$$

All coordinate variables, velocity components, and pressure are nondimensionalized by the cylinder diameter d and the freestream velocity u_∞ and ρu_∞^2, respectively. The time is normalized by d/u_∞.

Equations (1) and (2) are rewritten in a conservative form in generalized coordinates. The dependent variables in the transformed Navier–Stokes equations are volume fluxes across the faces of the cells, which are equivalent to using the contravariant velocity components on a staggered grid multiplied by the Jacobian of the coordinate transformation. Using this choice, the discretized mass conservation can be easily satisfied.[10,11] The terms in the transformed equations are described in detail in Ref. 11.

The integration method used to solve the transformed equations is based on a fully implicit, fractional step method.[11,12] All terms including cross-derivative diffusion terms are advanced with the Crank–Nicolson method in time and are resolved with the second-order central-difference scheme in space. A Newton method is used to solve the discretized nonlinear equation.

The flow geometry and coordinate system are shown in Fig. 1. We use a C-grid system. The periodic boundary condition is used

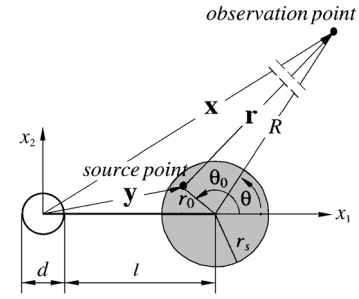

Fig. 1 Flow geometry and the coordinate system.

at the branch cut, and a convective outflow condition is used for the outflow boundary condition,[13] which allows vortices to smoothly pass away from the computational domain. A Dirichlet boundary condition, $u_1 = 1$, $u_2 = 0$, is used at far-field boundaries, and the no-slip condition is applied both on the cylinder wall and on the splitter plate.

The computational domain used is $-50 < x_1 < 100$ and $-50 < x_2 < 50$, where $(x_1 = 0, x_2 = 0)$ corresponds to the center location of the cylinder. A nonuniform mesh of 576×121 points is created using a hyperbolic grid generation technique. There are 64 grid points located on the cylinder surface. The current mesh and domain size have been determined from an extensive study of the numerical parameters, e.g., computational domain size, number of grid points, skewness of the computational mesh, etc. We have found that the domain size in the x_2 direction is more critical in accurately predicting the Strouhal number than the domain size in the streamwise x_1 direction. Doubling the domain size in both directions changed the predicted Strouhal number by less than 0.5%. To avoid a spurious sound caused by an active flux at the exit boundary,[14] we expand the outflow boundary up to $x_1 = 100$ to contain all of the noise sources (see Sec. IV.B).

For all cases investigated, we have used the computational time step $\Delta t = 0.02$. About three Newton iterations were needed to solve the discretized nonlinear momentum equations. We have also simulated the flow with $\Delta t = 0.01$, which resulted in less than 1% changes of the noise source functions. The CPU time required was about 2 s per time step using Cray YMP C90.

III. Acoustic Analogy

From the Lighthill acoustic analogy,[6] the concentrated unsteady flow region is the aeroacoustic source region, which can be obtained from an incompressible flow simulation. This incompressible flow approach can be justified from the compressibility effect of $\mathcal{O}(M^2)$ at a low Mach number. The governing equation for an acoustic wave propagation can be written in the following form:

$$\frac{\mathrm{D}^2 \rho}{\mathrm{D}t^2} - \frac{1}{M^2} \frac{\partial^2 \rho}{\partial x_j \partial x_j} = \frac{\partial^2 T_{ij}}{\partial x_i \partial x_j} \tag{3}$$

where

$$T_{ij} = \rho u_i' u_j' + \delta_{ij}[p - (\rho/M^2)] - \tau_{ij} \tag{4}$$

$$\tau_{ij} = \frac{1}{Re}\left(\frac{\partial u_i'}{\partial x_j} + \frac{\partial u_j'}{\partial x_i} - \frac{2}{3}\delta_{ij}\frac{\partial u_k'}{\partial x_k}\right) \tag{5}$$

$$\frac{\mathrm{D}}{\mathrm{D}t} = \frac{\partial}{\partial t} + \frac{\partial}{\partial x_1} \tag{6}$$

$$u_i' = u_i - \delta_{i1} \tag{7}$$

Equation (3) is a restatement of the Lighthill equation in terms of the values relative to the freestream values. Equation (4) is the Lighthill stress tensor composed of three terms, and Eq. (5) is the viscous part of the Stokes stress tensor.

When the reference frame is fixed on the moving solid boundary, Curle's solution of the Lighthill acoustic analogy can be applied. Also, in the case that the distance between observation and source points is larger than the acoustic wavelength, the far-field approximation can be applied. Furthermore, when the solid body and the source region are smaller than the typical wavelength, the source

region can be regarded as a compact source region. The acoustic density at the far field produced from a compact source region is approximated by

$$\rho_c(\boldsymbol{x},t)-1=\frac{M^3}{2\pi}\frac{x_i}{x}\int_0^\infty\frac{\partial}{\partial t^*}\int_{\partial\Omega}n_jP_{ij}(\boldsymbol{y},t^*)\,\mathrm{d}\boldsymbol{y}\,\mathrm{d}\xi$$
$$+\frac{M^4}{2\pi}\frac{x_ix_j}{x^2}\int_0^\infty\frac{\partial^2}{\partial t^{*2}}\int_\Omega T_{ij}(\boldsymbol{y},t^*)\,\mathrm{d}^2\boldsymbol{y}\,\mathrm{d}\xi \tag{8}$$

Although the original Curle's solution is derived in three-dimensional space,[7] the simulated flowfield in this study is a two-dimensional one, so that the two-dimensional version of Curle's solution is shown. Mitchell et al.[15] computed the far-field sound generated from a compressible corotating vortex pair using the same formulation and showed that the predicted sound agrees well with that obtained from a direct numerical simulation technique. A more general solution to Curle's solution for an acoustic wave propagation generated by a solid surface moving through a flowfield was considered by Ffowcs Williams and Hawkings.[16]

Equation (8) includes two typical noise source functions: a surface dipole and a volume quadrupole, which are generated from the surface of a cylinder and the entire unsteady flow region, respectively. The Mach number dependence of the volume quadrupole is $\mathcal{O}(M)$ times larger than that of the surface dipole. Here $\dot{D}_i$ and $\ddot{Q}_{ij}$ are the dipole and quadrupole source functions, respectively,

$$\dot{D}_i(t)=\int_0^\infty\frac{\partial}{\partial t^*}\int_{\partial\Omega}n_jP_{ij}(\boldsymbol{y},t^*)\,\mathrm{d}\boldsymbol{y}\,\mathrm{d}\xi \tag{9}$$

$$\ddot{Q}_{ij}(t)=\int_0^\infty\frac{\partial^2}{\partial t^{*2}}\int_\Omega T_{ij}(\boldsymbol{y},t^*)\,\mathrm{d}^2\boldsymbol{y}\,\mathrm{d}\xi \tag{10}$$

Next we consider the scattering effect of an incident sound field near the edge of the splitter plate. The scattering generated by an incident sound field at a rigid half-plane is governed by the Helmholtz equation:

$$\left(\frac{\partial^2}{\partial x_j\partial x_j}+k^2\right)\hat{G}(\boldsymbol{x},\boldsymbol{y},\omega)=-\delta(\boldsymbol{x},\boldsymbol{y}) \tag{11}$$

A two-dimensional solution of Eq. (11) can be obtained by the Green's function method:

$$\rho_s(\boldsymbol{x},t)-1$$
$$=M^2\int_{\partial\Omega}n_jP_{ij}(\boldsymbol{y},t)\frac{\partial G}{\partial y_i}\,\mathrm{d}\boldsymbol{y}+M^2\int_\Omega T_{ij}(\boldsymbol{y},t)\frac{\partial^2G}{\partial y_i\partial y_j}\,\mathrm{d}^2\boldsymbol{y} \tag{12}$$

The half-plane Green's function of Eq. (11) can be obtained by the Wiener–Hopf technique.[8,17] By putting this Green's function into Eq. (12), we obtain the scattering acoustic density. The scattered acoustic density by the distribution of quadrupoles near the edge can be expressed in the following form:

$$\rho_s(\boldsymbol{x},t)-1=\frac{M^2}{4\pi}\frac{1}{\sqrt{R}}\sin\frac{\theta}{2}\int_\Omega\left[([T_{11}]-[T_{22}])\sin\frac{3\theta_0}{2}\frac{1}{r_0\sqrt{r_0}}\right.$$
$$\left.-2[T_{12}]\cos\frac{3\theta_0}{2}\frac{1}{r_0\sqrt{r_0}}\right]\mathrm{d}^2\boldsymbol{y}\equiv\frac{M^2}{4\pi}\frac{1}{\sqrt{R}}\sin\frac{\theta}{2}Q_s \tag{13}$$

where $[T_{11}]$, $[T_{22}]$, and $[T_{12}]$ are the Reynolds stresses evaluated at the retarded time $t-MR$; and R, θ, θ_0 and r_0 are shown in Fig. 1. As opposed to the three-dimensional case,[8,9,18] the U^5 proportionality does not appear in the two-dimensional case, whereas the $\sin^2(\theta/2)$ directivity pattern holds here.

IV. Results

A. Flowfield

Near-field flow simulations were performed at $Re=100$ and 160, respectively, with and without splitter plates. The Strouhal number and drag variations due to splitter plates are identical to those in Ref. 5: At both Reynolds numbers, the Strouhal number decreases rapidly when $l<d$ (Fig. 2). On the other hand, the Strouhal number decreases slowly for $l>d$ at $Re=100$, whereas at $Re=160$, it reaches a local maximum near $l=2d$ and then decreases as the plate length further increases.

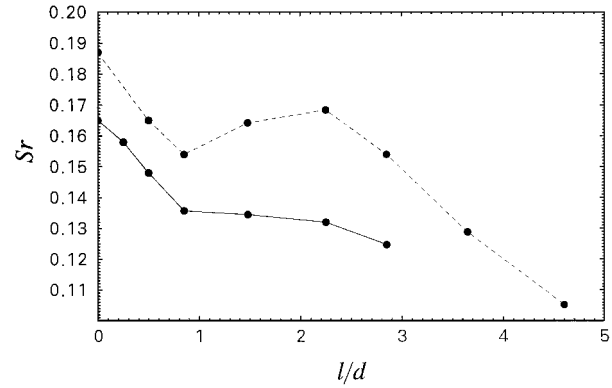

Fig. 2 Variation of the Strouhal number with the length of the splitter plate: ——, *Re* = 100, and - - - -, *Re* = 160.

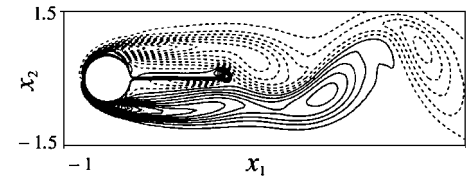

Fig. 3 Contour of the vorticity at *Re* = 160 with *l* = 2*d*. Contour levels are from − 19.28 to 19.28 with increments of 0.4: - - - -, negative values.

The reason that the Strouhal number increases for $l>d$ at $Re=160$ was investigated by Kwon and Choi.[5] They observed generation of the strong secondary vortex at the tip of the splitter plate in the cases of $l>d$ for $Re\geq120$. Figure 3 shows an instantaneous flowfield with the splitter plate of $l=2d$ at $Re=160$. When $l=2d$, there appears a strong secondary vortex at the tip of the plate, which has a sign opposite that of the main vortex. The size of the secondary vortex is much smaller than that of the main vortex. However, the strength of the secondary vortex is as large as that of the main vortex. Hence, the interaction between the main and secondary vortices is as active as the interaction between the main vortices, which causes an increase in the Strouhal number for $1<l/d<2$. In the case of $l=3d$, the role of the secondary vortex is relatively weak because of its longer distance from the cylinder, resulting in the decreased Strouhal number. This strong secondary vortex does not appear when $l=d$ at the same Reynolds number. Examination of instantaneous flowfields at $Re=100$ does not also reveal any strong secondary vortex at the tip of the plate in the cases of $1\leq l/d\leq3$.

B. Noise Source Components

At a low Mach number, the most dominant factors as noise sources are the temporal variations of drag and lift on the surface of a cylinder. Especially, when a splitter plate is attached, those factors rapidly change. Because temporal variations of drag and lift are caused by the fluctuations of the pressure and viscous skin friction, which are indeed generated by periodic vortex shedding behind the cylinder, noise sources can be effectively controlled by controlling vortex shedding using a splitter plate.

Figures 4a and 4b show the variation of drag and lift with respect to the length of the splitter plate at $Re=100$ and 160, respectively. In the case of $Re=100$, both the mean drag and amplitudes of drag and lift fluctuations decrease monotonically with the length of the splitter plates, so that the drag and lift dipoles monotonically decrease with the plate length (Fig. 5a). In the case of $Re=160$, however, although the mean value of drag monotonically decreases with the length of the splitter plate, the amplitudes of drag and lift fluctuations are smallest at $l=d$ (Fig. 4b), resulting in the smallest dipole source functions at $l=d$ (Fig. 5b). Interestingly, the lift fluctuations and lift dipole at $l=3d$ are larger than those without the splitter plate, due to the secondary vortex at the tip and also due to the large plate size subject to the vortex shedding motion in the wake. Note that the

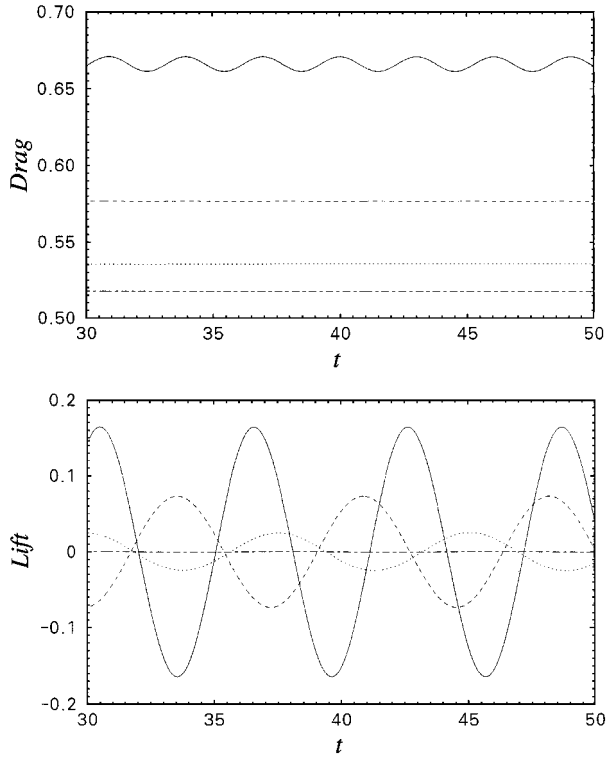

a) $Re = 100$

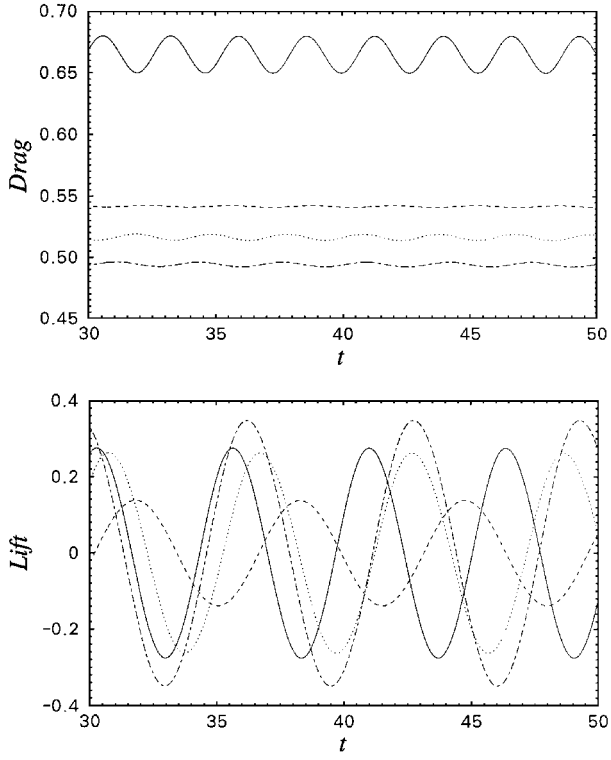

b) $Re = 160$

Fig. 4 Variation of drag and lift on the surface of the cylinder and splitter plate with the length of the splitter plate: ——, no plate; - - - -, $l = d$; · · · ·, $l = 2d$; and – – –, $l = 3d$.

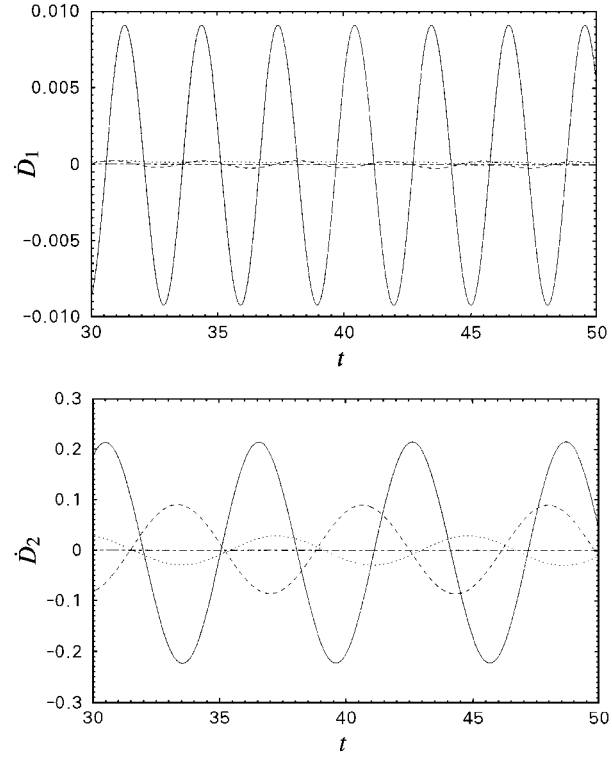

a) $Re = 100$

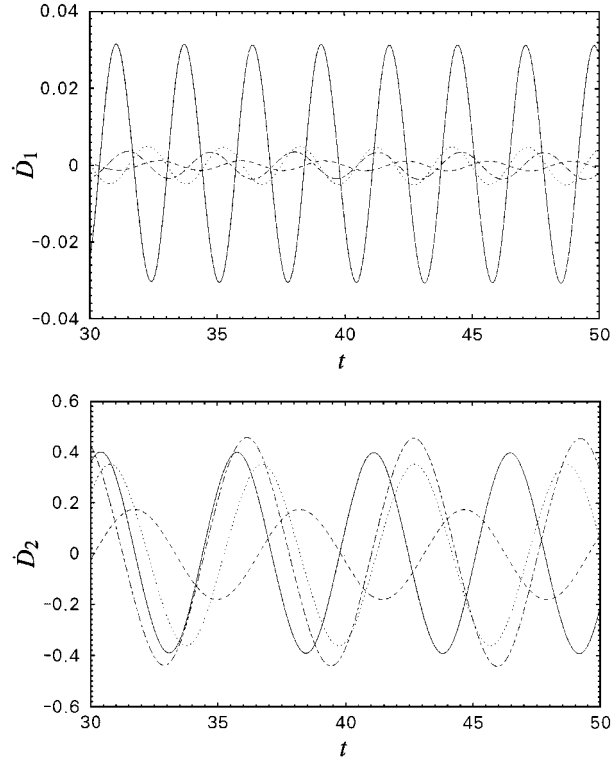

b) $Re = 160$

Fig. 5 Drag and lift dipoles $\dot{D}_i$: ——, no plate; - - - -, $l = d$; · · · ·, $l = 2d$; and – – –, $l = 3d$.

lift dipole is much larger than the drag dipole at all cases considered and, thus, contributes most of the total dipole.

The Lighthill stress tensor in Eq. (4) is usually approximated by the Reynolds stress term only.[6,14,19] The volume quadrupole noise source function can be obtained by the second time derivative of the Reynolds stresses [Eq. (10)]. When the computation domain is not large enough to contain all of the active noise sources, a spurious sound is produced at the exit boundary, and it contaminates the original noise source. Wang et al.[14] suggested a scheme to correct a spurious sound caused by eddies crossing the exit boundary. Their scheme worked very well for $\ddot{Q}_{11}$ and $\ddot{Q}_{12}$ but not for $\ddot{Q}_{22}$. Therefore, in this study, we simply extended the computational domain size in the streamwise direction from $50d$ to $100d$ behind the cylinder without any correction scheme. It was found that the quadrupoles were identical when the domain size behind the cylinder was larger than $80d$. Figures 6a and 6b show the variation of the quadrupole source functions with the length of the splitter plate at $Re = 100$ and

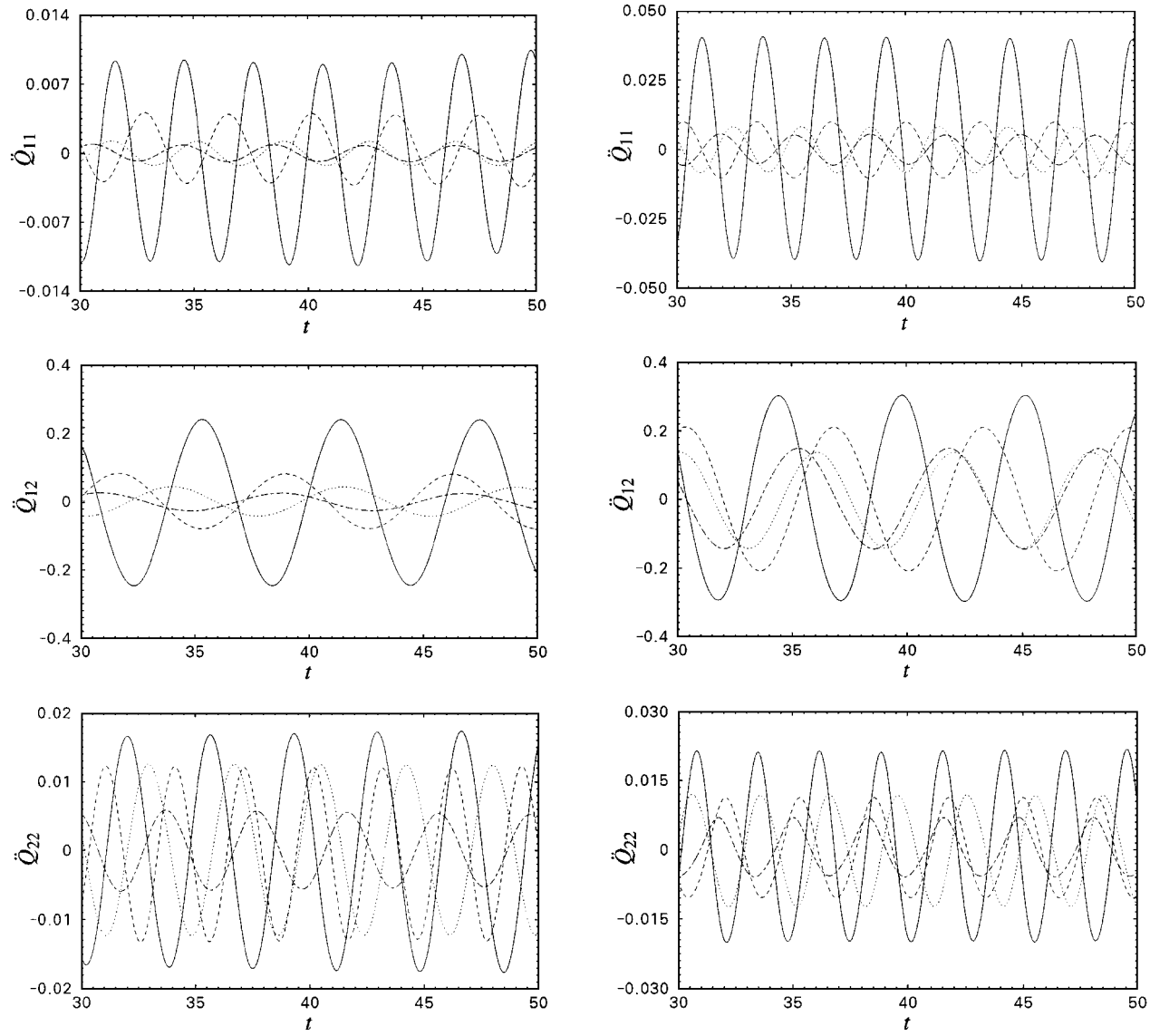

Fig. 6 Quadrupoles $\ddot{Q}_{ij}$: ——, no plate; - - - -, $l = d$; · · · ·, $l = 2d$; and – – –, $l = 3d$.

160, respectively. All quadrupoles decrease when a splitter plate is attached. It is also shown that, for all of the cases investigated, the dominant quadrupole is $\ddot{Q}_{12}$ caused by the Reynolds shear stress fluctuations.

The volume quadrupole contribution to a total acoustic density propagation is $\mathcal{O}(M^4)$, whereas the surface dipole contribution is $\mathcal{O}(M^3)$. Thus, the effect of the quadrupole source on the far-field acoustic density fluctuations is smaller than that of the dipole source at a low Mach number, and thus, the contribution of the lift dipole is dominant for the total acoustic field, $\rho_c - 1$, for all of the cases of $Re = 100$ and 160. Figure 7 shows the acoustic density propagation at a far-field location, x_1 and $x_2 = 1000$, at $M = 0.01$. It is shown that at $Re = 100$ the total acoustic density monotonically decreases with the increased plate length, whereas at $Re = 160$ it is smallest at $l = d$ and is largest at $l = 3d$ due to the increase in the lift dipole (Fig. 5b). The value at $l = 3d$ is larger than that without the splitter plate.

In the case of $Re = 100$, because the dipoles rapidly decrease, the contribution of the volume quadrupoles to the total acoustic field, $\rho_c - 1$, gradually increases with the length of the splitter plate (Figs. 5a and 6a). Thus, the role of the volume quadrupoles becomes more important as the length of the splitter plate increases. Figures 8a and 8b show contours of the far-field acoustic density at $Re = 100$ and $M = 0.01$ without and with the splitter plate of $l = 3d$, respectively. It is clear that the total acoustic field shows the dipole characteristics when there is no splitter plate, whereas the quadrupole characteristics appear in the total acoustic field in the case of $l = 3d$. In the case of $Re = 160$, however, the lift dipole increases when $l > d$ and is much larger than the volume quadrupoles (Figs. 5b and 6b). Hence, the total acoustic density field at $Re = 160$ shows the dipole characteristics in all of the cases examined.

C. Scattering Effect

In this section, we consider a scattering effect at the edge of a splitter plate because it is known that a significant amount of sound is generated by eddies located very near the sharp edge. It was shown that a strong secondary vortex was generated at the edge of the plates of $l = 2d$ and $3d$ at $Re = 160$. This secondary vortex may be a source of the scattering noise in this flow.

We estimate the strength of the scattering noise source due to the secondary vortex at the edge of the plate by increasing the integration domain (see Fig. 1), i.e.,

$$Q_s = \int_0^{r_s}\int_0^{2\pi}\left[([T_{11}] - [T_{22}])\sin\frac{3\theta_0}{2}\frac{1}{r_0\sqrt{r_0}} - 2[T_{12}]\cos\frac{3\theta_0}{2}\frac{1}{r_0\sqrt{r_0}}\right] r_0\,\mathrm{d}\theta_0\,\mathrm{d}r_0 \tag{14}$$

Note that the region of the scattering sound source should be smaller than the length of the plate for Eq. (13) to be valid. Figure 9 shows

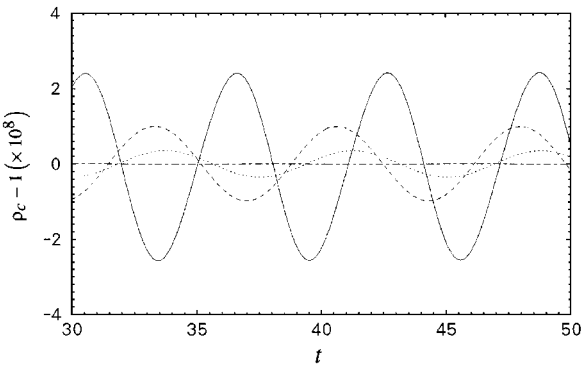

a) $Re = 100$

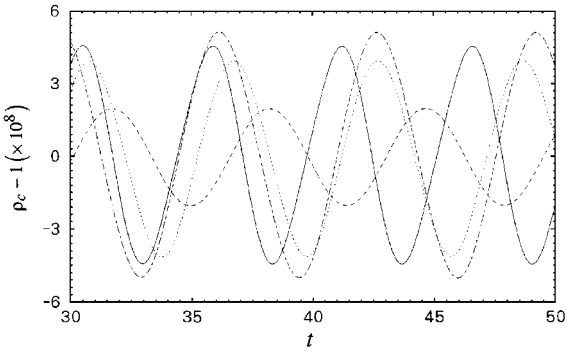

b) $Re = 160$

Fig. 7 Acoustic density fluctuations at the location ($x_1 = 1000, x_2 = 1000$) with $M = 0.01$: ——, no plate; - - - -, $l = d$; · · · ·, $l = 2d$; and – – –, $l = 3d$.

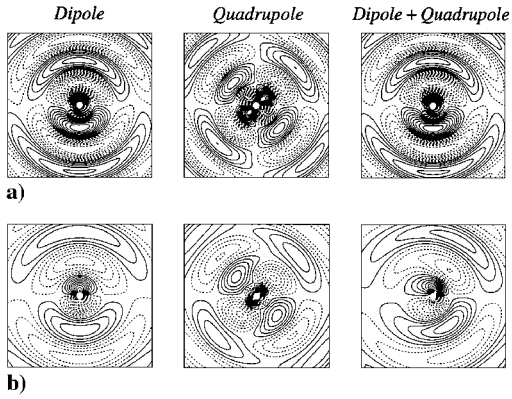

Fig. 8 Contours of the acoustic density fluctuations at $Re = 100$ and $M = 0.01$; far-field domain size is $-1000 \le x_1, x_2 \le 1000$. Maximum values of the dipole and quadrupole density fluctuations and their sum are, respectively, a) 4.25×10^{-8}, 3.21×10^{-10}, and 4.25×10^{-8}; no plate; and b) 8.14×10^{-11}, 4.38×10^{-11}, and 1.0×10^{-10}; $l = 3d$.

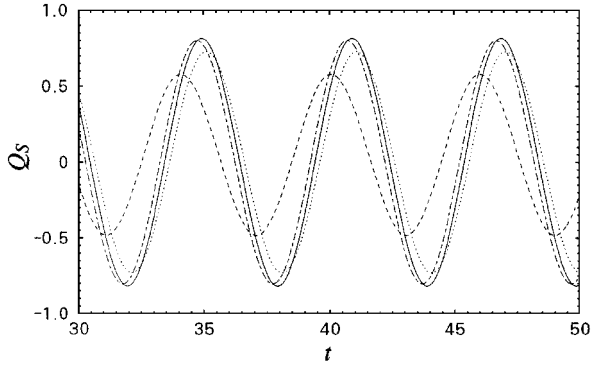

Fig. 9 Scattering source near the edge of the splitter plate at $Re = 160$ and $l = 2d$: - - - -, $r_s = 0.5$; · · · ·, $r_s = 1$; – – –, $r_s = 1.5$; and ——, $r_s = 50$.

the variation of Q_s at $l = 2d$ and $Re = 160$ as the integration domain, i.e., r_s, increases. It shows that there is little variation of Q_s when $r_s \ge 1$, indicating that an important source of the scattering sound is located very near the edge of the plate, which apparently satisfies the assumption of Eq. (13). Note that the magnitude of the scattering noise source is nonnegligible, as compared to the dipole and quadrupole sources shown in Figs. 5b and 6b. Direct comparison of $\rho_s - 1$ with $\rho_c - 1$ at a far-field location is not straightforward because Eq. (13) is derived for a half-infinite plate. A rough estimation of $\rho_s - 1$ at ($x_1 = 1000$, $x_2 = 1000$) showed that the scattering noise is bigger than the dipole and quadrupole noise. Because the scattering noise contribution to the total acoustic density is proportional to $O(M^2)$ and is inversely proportional to $\sqrt{R}$ [Eq. (13)], the scattering sound becomes more important at low Mach numbers and less effective at the far field.

V. Summary

Laminar vortex shedding behind a circular cylinder with and without splitter plates attached to the cylinder base at the Reynolds numbers of 100 and 160 was simulated by solving the unsteady two-dimensional incompressible Navier–Stokes equations. The Strouhal number, lift, and drag rapidly changed with the length of the splitter plate. The acoustic source functions from vortex shedding behind the cylinder were computed using the Lighthill acoustic analogy and Curle's solution of the Lighthill equation.

In the case of no splitter plate, the volume quadrupole noise was small at a low Mach number, compared with the surface dipole noise from the cylinder. It was also shown that the dominant noise source was the lift dipole. When the splitter plate was attached to the cylinder, there were significant modifications of the noise sources. In the case of $Re = 100$, as the length of the plate increased, the dipoles rapidly decreased, but the quadrupoles gradually decreased with the length of the splitter plate. Thus, the contribution of the quadrupole source to the total acoustic field gradually increased as the plate length increased. On the other hand, in the case of $Re = 160$, the lift dipole decreased when $l \le d$ and then increased for $l > d$ due to a strong secondary vortex at the tip of the plate. The lift dipole at $l = 3d$ was larger than that with no splitter plate. All quadrupoles decreased when the splitter plate was attached, and thus, the lift dipole was most dominant among all of the noise sources at $Re = 160$.

A strong secondary vortex was generated at the edge of the splitter plates of $l = 2d$ and $3d$ at $Re = 160$. Thus, the scattering effect at the edge of the plate was considered using the half-plane Green's function method. It was shown that the magnitude of the scattering noise source was nonnegligible, as compared to the dipole and quadrupole sources.

Acknowledgments

This work was sponsored by the Korea Science and Engineering Foundation under Contract 961-1009-075-2. The use of the supercomputer facilities from the Systems Engineering Research Institute, Taejon, Republic of Korea, is also appreciated.

References

[1] Gerrard, J. H., "The Mechanics of the Formation Region of Vortices Behind Bluff Bodies," *Journal of Fluid Mechanics*, Vol. 25, 1966, pp. 401–413.

[2] Apelt, C. J., West, G. S., and Szewczyk, A. A., "The Effects of Wake Splitter Plates on the Flow Past a Circular Cylinder in the Range $10^4 < R < 5 \times 10^4$," *Journal of Fluid Mechanics*, Vol. 61, 1973, pp. 187–198.

[3] Apelt, C. J., and West, G. S., "The Effects of Wake Splitter Plates on Bluff-Body Flow in the Range $10^4 < R < 5 \times 10^4$: Part 2," *Journal of Fluid Mechanics*, Vol. 71, 1975, pp. 145–160.

[4] Cimbala, J. M., and Garg, S., "Flow in the Wake of a Freely Rotatable Cylinder with Splitter Plate," *AIAA Journal*, Vol. 29, No. 6, 1991, pp. 1001–1003.

[5] Kwon, K., and Choi, H., "Control of Laminar Vortex Shedding Behind a Circular Cylinder Using Splitter Plates," *Physics of Fluids*, Vol. 8, No. 2, 1996, pp. 479–486.

[6] Lighthill, M. J., "On Sound Generated Aerodynamically: I. General Theory," *Proceedings of the Royal Society of London, Series A: Mathematical and Physical Sciences*, Vol. 211, No. 1107, 1952, pp. 564–587.

[7] Curle, N., "The Influence of Solid Boundaries upon Aerodynamic Sound," *Proceedings of the Royal Society of London, Series A: Mathematical and Physical Sciences*, Vol. 231, No. 1187, 1955, pp. 505–514.

[8]Crighton, D. G., and Leppington, F. G., "Scattering of Aerodynamic Noise by a Semi-Infinite Compliant Plate," *Journal of Fluid Mechanics*, Vol. 43, Pt. 4, 1970, pp. 721–736.

[9]Crighton, D. G., and Leppington, F. G., "On the Scattering of Aerodynamic Noise," *Journal of Fluid Mechanics*, Vol. 46, Pt. 3, 1971, pp. 577–597.

[10]Rosenfeld, M., Kwak, D., and Vinokur, M., "A Fractional Step Solution Method for the Unsteady Incompressible Navier–Stokes Equations in Generalized Coordinate Systems," *Journal of Computational Physics*, Vol. 94, No. 1, 1991, pp. 102–137.

[11]Choi, H., Moin, P., and Kim, J., "Turbulent Drag Reduction: Studies of Feedback Control and Flow over Riblets," Dept. of Mechanical Engineering, Rept. TF-55, Stanford Univ., Stanford, CA, Sept. 1992.

[12]Choi, H., and Moin, P., "Effects of the Computational Time Step on Numerical Solutions of Turbulent Flow," *Journal of Computational Physics*, Vol. 113, No. 1, 1994, pp. 1–4.

[13]Pauley, L. L., Moin, P., and Reynolds, W. C., "The Structure of Two-Dimensional Separation," *Journal of Fluid Mechanics*, Vol. 220, 1990, pp. 397–411.

[14]Wang, M., Lele, S. K., and Moin, P., "Computation of Quadrupole Noise Using Acoustic Analogy," *AIAA Journal*, Vol. 34, No. 11, 1996, pp. 2247–2254.

[15]Mitchell, B. E., Lele, S. K., and Moin, P., "Direct Computation of the Sound from a Compressible Co-Rotating Vortex Pair," *Journal of Fluid Mechanics*, Vol. 285, Feb. 1995, pp. 181–202.

[16]Ffowcs Williams, J. E., and Hawkings, D. L., "Sound Generation by Turbulence and Surfaces in Arbitrary Motion," *Philosophical Transactions of the Royal Society of London, Series A: Mathematical and Physical Sciences*, Vol. 264, No. 1151, 1969, pp. 321–342.

[17]Howe, M. S., "Contributions to the Theory of Aerodynamic Sound, with Application to Excess Jet Noise and the Theory of the Flute," *Journal of Fluid Mechanics*, Vol. 71, Pt. 4, 1975, pp. 625–673.

[18]Ffowcs Williams, J. E., and Hall, L. H., "Aerodynamic Sound Generation by Turbulent Flow in the Vicinity of a Scattering Half Plane," *Journal of Fluid Mechanics*, Vol. 40, Pt. 4, 1970, pp. 657–670.

[19]Wang, M., Lele, S. K., and Moin, P., "Sound Radiation During Local Laminar Breakdown in a Low-Mach-Number Boundary Layer," *Journal of Fluid Mechanics*, Vol. 319, 1996, pp. 197–218.

R. W. Wlezien
Associate Editor